

Effect of the Air Drag Perturbation in the Eccentricity Vector for Very Low Earth Orbits

Javier Sánchez¹ and André Vasconcelos²

¹ GMV at ESA/ESOC, Robert-Bosch-Str. 5, 64293, Darmstadt, Germany.
Telephone: +496151902416, E-mail: javier.sanchez@esa.int

² SCISYS at ESA/ESOC, Robert-Bosch-Str. 5, 64293, Darmstadt, Germany.
Telephone: +496151902235, E-mail: andre.vasconcelos@esa.int

Abstract

Earth's potential perturbation results in a strong eccentricity vector disturbance for Earth observation missions. In order to achieve a stable eccentricity control Earth observation missions are usually designed selecting an eccentricity vector close to the so-called frozen eccentricity point. However, eccentricity control close to the frozen eccentricity is subject to other perturbation forces. Besides the effect of the Solar Radiation Pressure (SRP), which has been characterized in previous works [1] [2], the present paper tackles eccentricity changes induced by the effect of the air drag. These eccentricity changes are originated by a non-uniform distribution of the air density along the orbit, and are specially relevant in very low Earth orbits. The results also encompass a comparison of the disturbances in the eccentricity vector caused by air drag and SRP for different orbit types, as a function of their altitude and orbital plane orientation.

Keywords: Eccentricity control, Altitude control, Frozen eccentricity, Air drag, Solar Radiation Pressure

Introduction

The study presented in this paper is an extension of previous work modelling the long-periodic changes in eccentricity for Earth observation missions [1] [2]. This modelling, rather than providing an accurate prediction of the eccentricity vector, aims at extracting the value from understanding its behaviour in the presence of the many different perturbations. This enables the design of effective eccentricity control strategies, the simplification of Flight Dynamics operations or an easy evaluation of requirements compliance during mission design.

Earth observation missions are typically designed with their eccentricity vector at the frozen eccentricity point. The frozen eccentricity is an equilibrium point, which is derived from the dynamics of the eccentricity vector under the effect of the Earth's potential perturbation. In absence of any other perturbation, the motion in the vicinity of the frozen eccentricity point can be modelled as a rotation of the eccentricity vector around the frozen eccentricity. The angular velocity of this motion depends on the orbit characteristics. Namely, the semi-major axis, the inclination and the eccentricity itself. Nevertheless, once the orbit of a given mission has been fixed at design level, the typical orbital changes taking place throughout the life of an Earth observation mission are small enough, so that the value of this angular velocity can be assumed to be nearly constant [3] [5].

The effect of the SRP perturbation is clearly visible when controlling the eccentricity vector close to the frozen eccentricity. The reason for this resides in the fact that at the frozen eccentricity the perturbation from the Earth's potential nullifies, and the eccentricity vector dynamics are therefore dominated by all other perturbations which come next in relative

importance. For a nearly circular orbit, the scalar product of the velocity vector with the projection of the SRP force onto the orbital plane follows an asymmetric distribution along the orbit. This configuration is specially effective in producing eccentricity variations, and is the reason why for a wide range of Earth observation orbits the SRP perturbation plays an important role in the eccentricity vector behaviour.

Combining the Earth's potential effect with that from the SRP the eccentricity vector dynamics can be modelled as the composition of two different motions [1]: A rotation of the eccentricity vector around the frozen eccentricity point, caused by the Earth's potential perturbation; and an eccentricity vector change rate, in a direction perpendicular to the Sun's direction projection onto the orbital plane (see Eqn 1), due to the effect of the SRP perturbation.

$$\dot{\vec{e}}_{SRP} = \frac{3p}{2h} \left[1 - \frac{\Delta\theta}{2\pi} + \frac{1}{3} \frac{\sin \Delta\theta}{2\pi} \right] \begin{pmatrix} 0 & 1 \\ -1 & 0 \end{pmatrix} \vec{v}_{SRP_{IP}} \quad (1)$$

Regarding the effect of the air drag, its contribution can be introduced as follows. If the magnitude of the air drag would be assumed constant along a circular orbit and in a direction opposite to the velocity vector, the net change in the eccentricity would be zero. However, in a real orbit, the action of the air drag on the velocity vector is not uniform due to changes in the air density along the orbit. These variations depend on several factors: the local time, altitude variations due to both, the shape of the Earth and the orbit eccentricity, and other seasonal changes [6].

The result of this non-uniform action of the air drag, integrated along an orbital revolution, leads to net variations in the eccentricity vector. For lower orbits, as the air density grows, these differences in distribution are magnified, and the effect on the eccentricity vector becomes larger. If the orbit is low enough, eccentricity changes caused by the air drag perturbation can reach the same order of magnitude than those caused by the SRP or even exceed it, as it will be shown in further sections. The purpose of this paper is to characterise these changes in eccentricity caused by the air drag perturbation, and to compare them against those consequence of the SRP. By comparing their orders of magnitude, the relative importance of each one of these perturbations can be determined, which allows identifying the scenarios where they have to be taken into account for a correct modelling.

The composition of a rotation around the frozen eccentricity point and an eccentricity vector change rate in a given direction can be understood establishing an analogy with planar rigid body motion [1] [2]. The position of the Instant Centre of Rotation (ICR) is given by Eqn 2. In this equation $\vec{\Omega}$ represents the angular velocity around the frozen eccentricity (constant), while $\dot{\vec{e}}_{PER}$ represents the eccentricity vector change rate caused by other perturbations. $\dot{\vec{e}}_{PER}$ is a function of time in a time scale much longer than the orbital period (i.e. seasonal), and it does not depend on the position of the eccentricity vector itself, at least within the range of interest, which is in the vicinity of the frozen eccentricity. In a general case, both, the air drag and the SRP perturbations, may contribute with significant eccentricity vector change rates to the $\dot{\vec{e}}_{PER}$ term.

$$\vec{r}_{ICR} = \frac{\vec{\Omega} \times \dot{\vec{e}}_{PER}}{\Omega^2} = \frac{\vec{\Omega} \times (\dot{\vec{e}}_{SRP} + \dot{\vec{e}}_{DRAG})}{\Omega^2} \quad (2)$$

Modelling the eccentricity vector changes caused by the air drag perturbation

Applying the Gauss form of the variational equations, the eccentricity change rate can be modelled as given in Eqn 3 and Eqn 4 as a function of a perturbing force $\vec{\gamma}$. Assuming the air drag as the perturbing force, Eqn 4 has been integrated along the orbital period. The air density model used for the computation of the air drag force is the NLRMSISE-00, combined with a numerical integration of the equation using the trapezoid rule. Independently, the contribution of the SRP force to the eccentricity vector change rate has also been computed using Eqn 4 for comparison purposes. For this, the IERS model [4] has been used, inserting it as perturbing force into Eqn 4 in an analogous way as it was done with the air drag.

The reason to choose a numerical integration method is due to the characteristics of the air drag effect on the eccentricity that have been advanced in the introduction. Eccentricity changes due to the air drag perturbation are caused by an uneven distribution of the air drag along the orbit. Hence, the interest of using a detailed atmospheric model for the analysis, which can be better treated numerically.

$$\dot{\vec{h}} = \vec{r} \times \vec{\gamma} \quad (3)$$

$$\dot{\vec{e}} = \frac{\dot{\vec{r}} \times \vec{h}}{\mu} + \frac{\vec{\gamma} \times \vec{h}}{\mu} \quad (4)$$

Throughout this paper, air drag and SRP forces have been computed assuming 1 m² reference surfaces, unitary air drag and SRP coefficients and a spacecraft mass of 1000 kg. In order to extrapolate the results to spacecraft with different characteristics the resulting eccentricity changes need to be properly scaled. The values integrated from Eqn 4 are projected onto the orbital plane. This is done so because, by definition, the eccentricity vector is contained within the orbital plane. The out-of-plane component of the eccentricity vector change rate contributes to the rotation of the orbital plane, not to the evolution of the eccentricity vector itself within the plane [1]. The integration is performed taking 240 integration steps along an orbital revolution. The result of the integration is a vector representing the eccentricity change accumulated after an orbital revolution. For the results shown hereinafter a scenario has been selected using as starting epoch the 1st of September 2002. The solar activity conditions at that epoch are intermediate to high, with solar activity indices of F10.7 = 181, M10.7 = 169 and Ap = 13.

The graph depicted in Fig. 1 shows the magnitude of the left-hand side of Eqn 4 as a function of the orbit position for a Sentinel-3-like orbit. Sentinel-3 is operated in a sun-synchronous orbit, with a local time of the ascending node at 22 hours and a ground track repeat cycle of 385 orbits in 27 days (orbital period: 100.987 minutes). The radius of the area represented in Fig. 1 for each orbital position is equal to the magnitude of the left-hand side of Eqn 4. This representation allows the identification of the areas along an orbit revolution with a higher contribution to the eccentricity change. It can be seen that the distribution in Fig. 1 is not balanced, with a higher contribution of the descending arc of the orbit. As a result of this a net eccentricity change can be inferred.

The integration of the eccentricity change along an orbit revolution has been represented in Fig. 2. The integration has been performed separately for eccentricity changes caused by air drag and SRP for comparison purposes. The data is displayed in logarithmic scale.

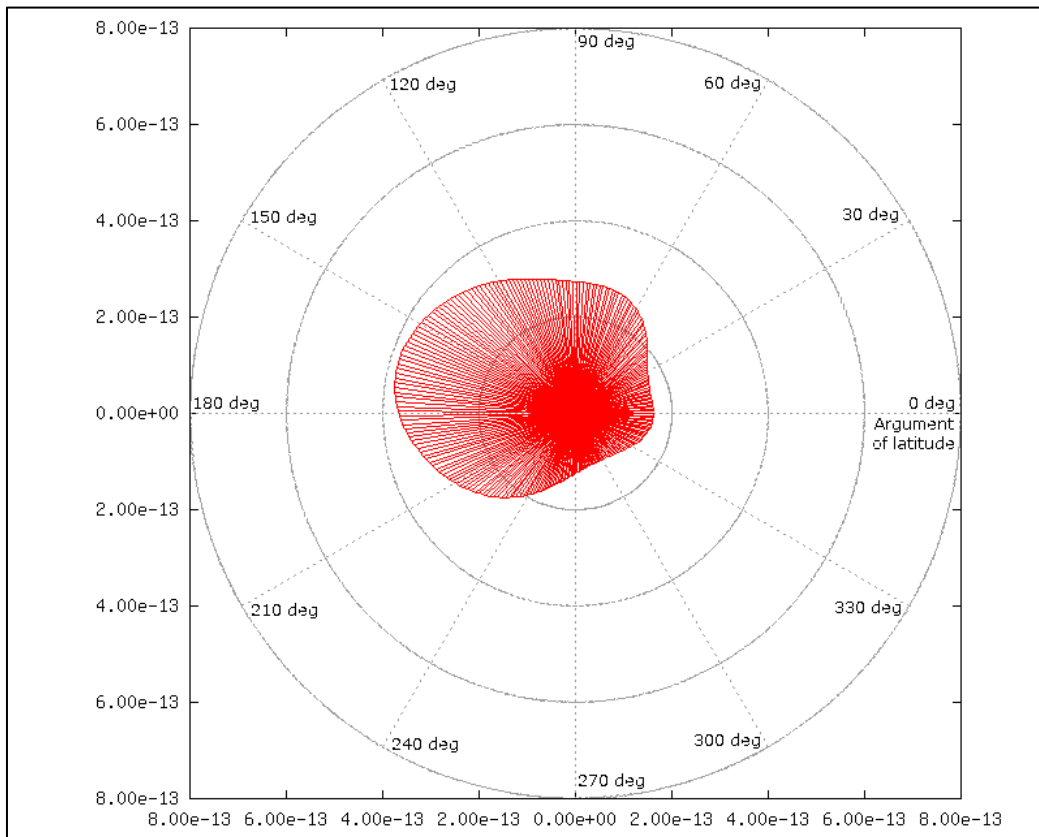


Fig. 1: Magnitude of the eccentricity vector change rate due to air drag for each integration step. Results computed for a Sentinel-3-like orbit.

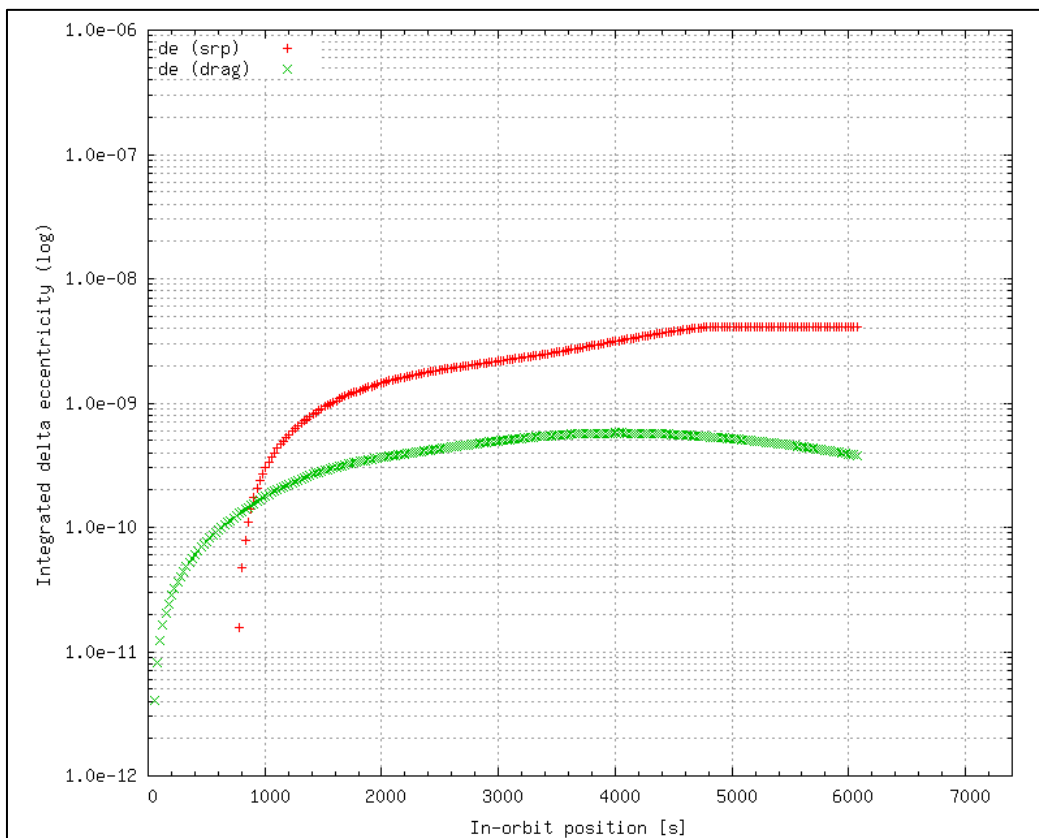


Fig. 2: Integration along an orbital revolution of the eccentricity change (magnitude) due to both, SRP and air drag perturbations. Results computed for a Sentinel-3-like orbit.

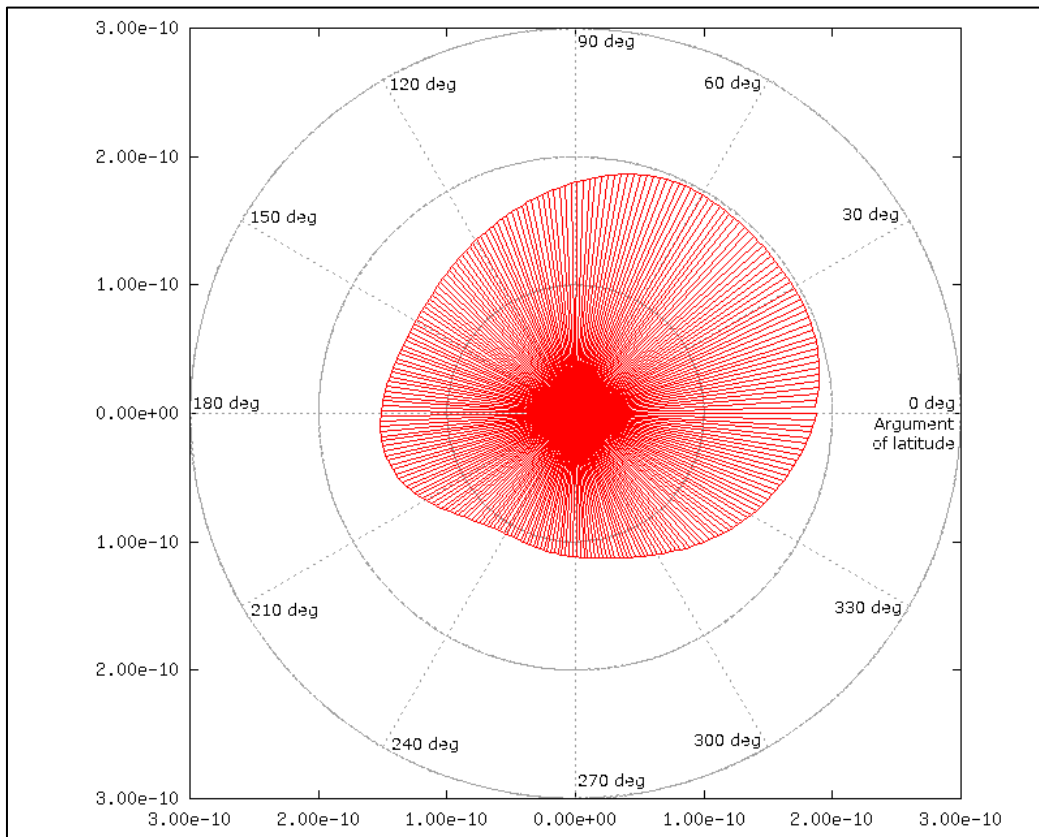


Fig. 3: Magnitude of the eccentricity vector change rate due to air drag for each integration step. Results computed for an Aeolus-like orbit.

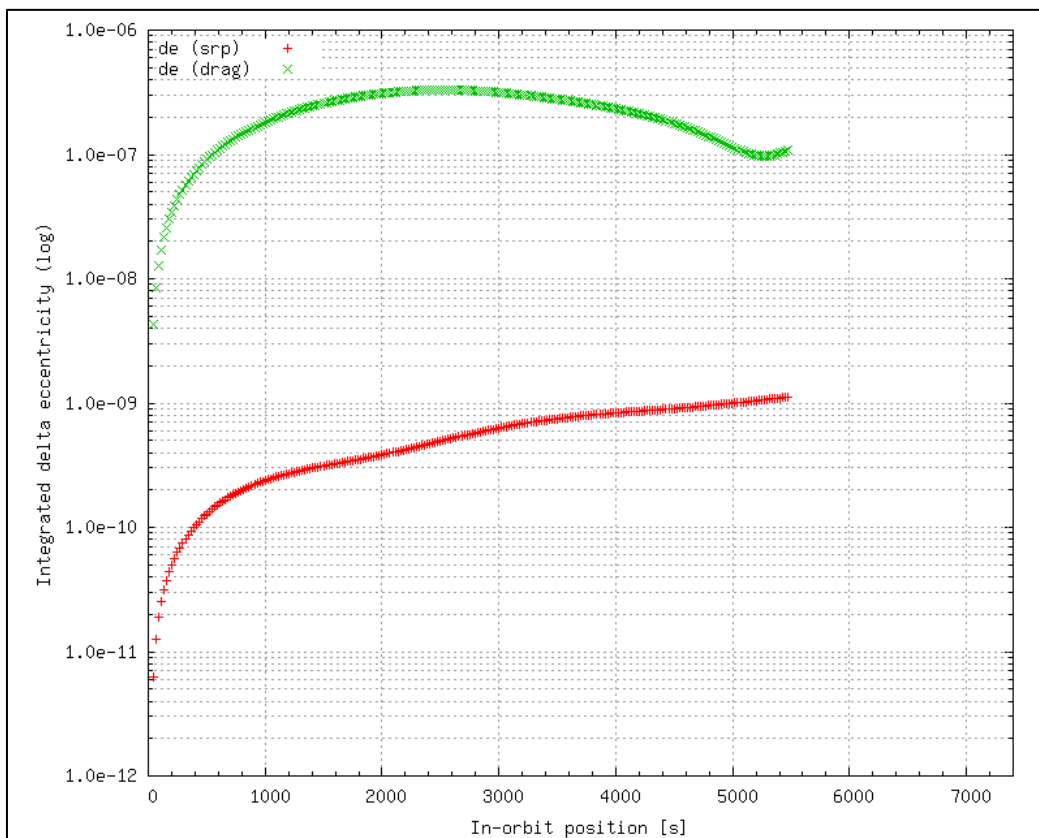


Fig. 4: Integration along an orbital revolution of the eccentricity change (magnitude) due to both, SRP and air drag perturbations. Results computed for an Aeolus-like orbit.

The results depicted in Fig. 3 and Fig. 4 have been obtained following the same process, but considering an orbit equivalent to that of the ESA Earth Explorer Aeolus. Aeolus is controlled following a sun-synchronous reference orbit, with a local time of the ascending node at 18 hours and a ground track repeat cycle of 111 orbits in 7 days, which leads to a very low orbital height (orbital period: 90.811 minutes). The resulting eccentricity change caused by the air drag perturbation is approximately 2 orders of magnitude higher than the one caused by the SRP perturbation, as it can be seen in Fig. 4.

Comparison of air drag and SRP influence in the eccentricity vector

Given the two perturbations, air drag and SRP, another important question is how strong is the relative effect of each one of them in the eccentricity vector, and what are the conditions under which the motion of the eccentricity vector is dominated by one of the perturbations or the other. The work presented in this section is aimed at that purpose. This type of analysis allows discriminating the conditions for which one of the perturbations can be disregarded in favour of the other, or to point out the scenarios in which both have to be taken into account in order to model the eccentricity vector behaviour with sufficient accuracy. The relative importance of each one of the perturbations has been evaluated computing the ratio given in Eqn 5.

$$r_{SRP/DRAG} = \frac{|\dot{e}_{SRP}|}{|\dot{e}_{DRAG}|} \quad (5)$$

Given an input trajectory the eccentricity change due to the action of the SRP is computed from Eqn 4 as indicated in the previous section. The resulting vector is then projected onto the orbital plane. Then, its magnitude is computed. The same process is followed taking the air drag as perturbing force in Eqn 4. Finally, the ratio defined in Eqn 5 is computed. These results have been used in order to create the heat map depicted in Fig. 5, as a function of the orbital period (i.e. semi-major axis) and local time. The range covered by the analysis spans from orbital periods from 88 to 120 minutes and local times from 0 to 23 hours. In order to do this a series of input orbits were generated. These input orbits were created as sun-synchronous orbits with a the orbital period and local time for each one of the cases.

The results plotted in Fig. 5 have been generated for the 1st of September 2002, assuming the solar activity indices reconstructed for that epoch, as given in the previous section. The colour scale in Fig. 5 is logarithmic and allows identifying the difference in orders of magnitude between the effect of one perturbation and the other. The data has been generated again assuming air drag and SRP reference surfaces of 1 m², unitary air drag and SRP coefficients and a spacecraft mass of 1000 kg. In order to extrapolate the results to a particular spacecraft the results read from the heat map have to be multiplied by the ratio of reference surfaces and coefficients defined in Eqn 6.

$$f_{SRP/DRAG} = \frac{S_{SRP} C_{SRP}}{S_{DRAG} C_D} \quad (6)$$

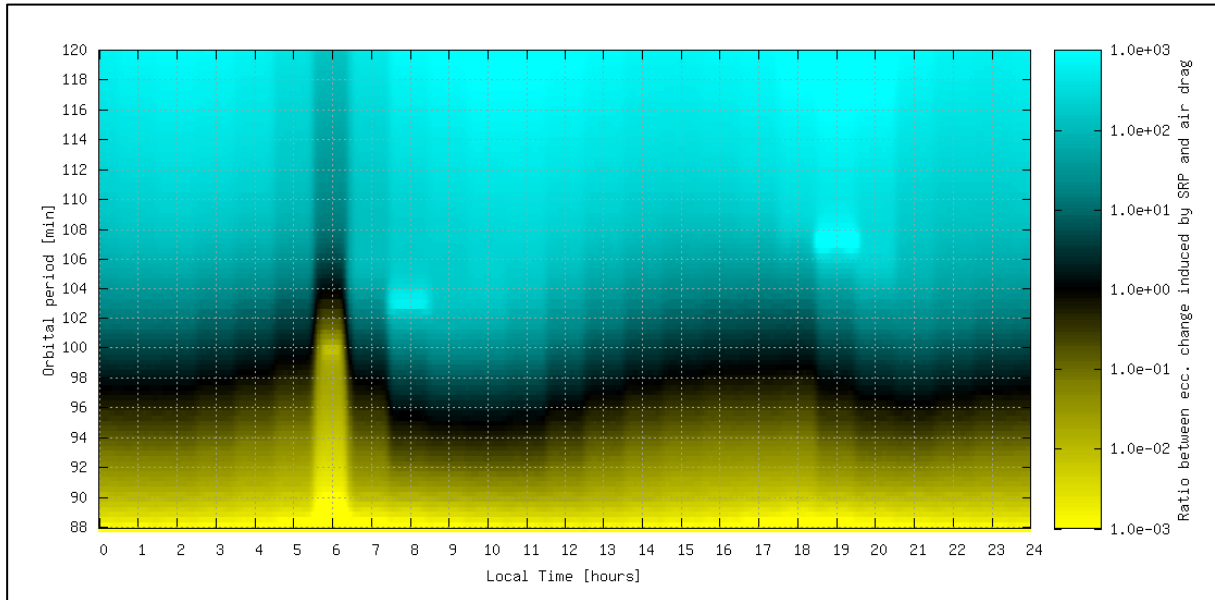


Fig. 5: Comparison of the eccentricity changes induced by air drag and SRP.

The data given in Fig. 5 has a strong dependency on solar activity levels. Fig. 6 and Fig. 7 show the results of the same type of results, but assuming high and low solar activity scenarios as defined by the European Cooperation for Space Standardization (ECSS), summarised in Table 1. The main consequence as the solar activity increases, from a qualitative point of view, is a displacement to higher orbital periods of the range where both perturbations have an effect of the same order of magnitude on the eccentricity vector (i.e. $r_{SRP/DRAG} = 1$).

Table 1: ECSS solar activity reference scenarios.

Scenario	F 10.7	M 10.7	Ap
High	250	250	45
Low	65	65	0

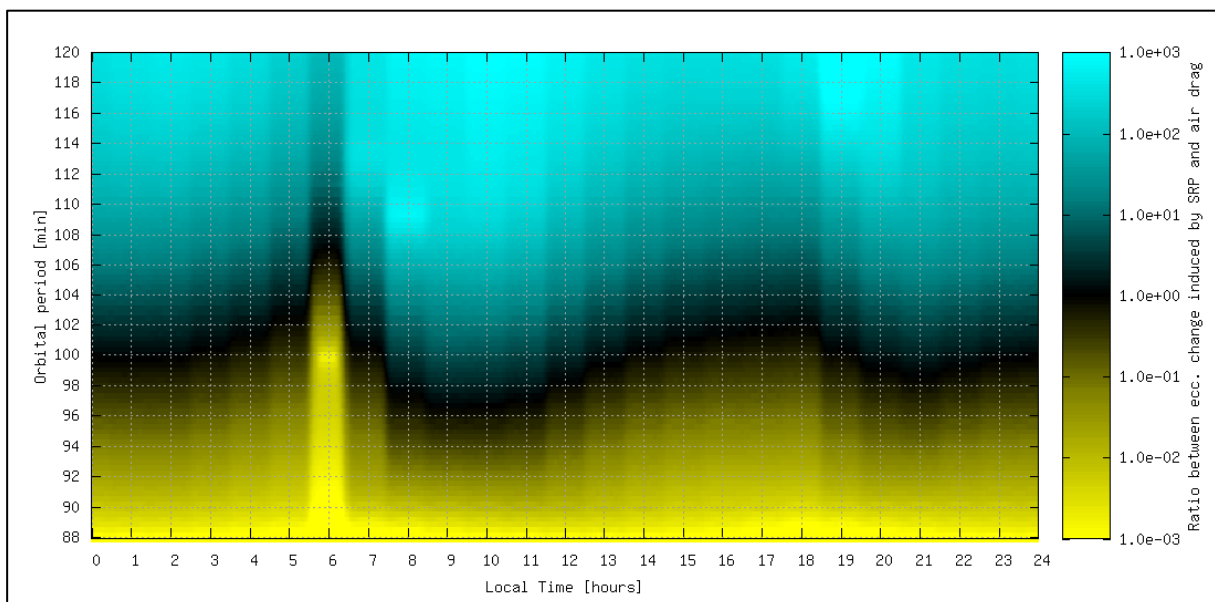


Fig. 6: Comparison of the eccentricity changes induced by air drag and SRP. High solar activity scenario.

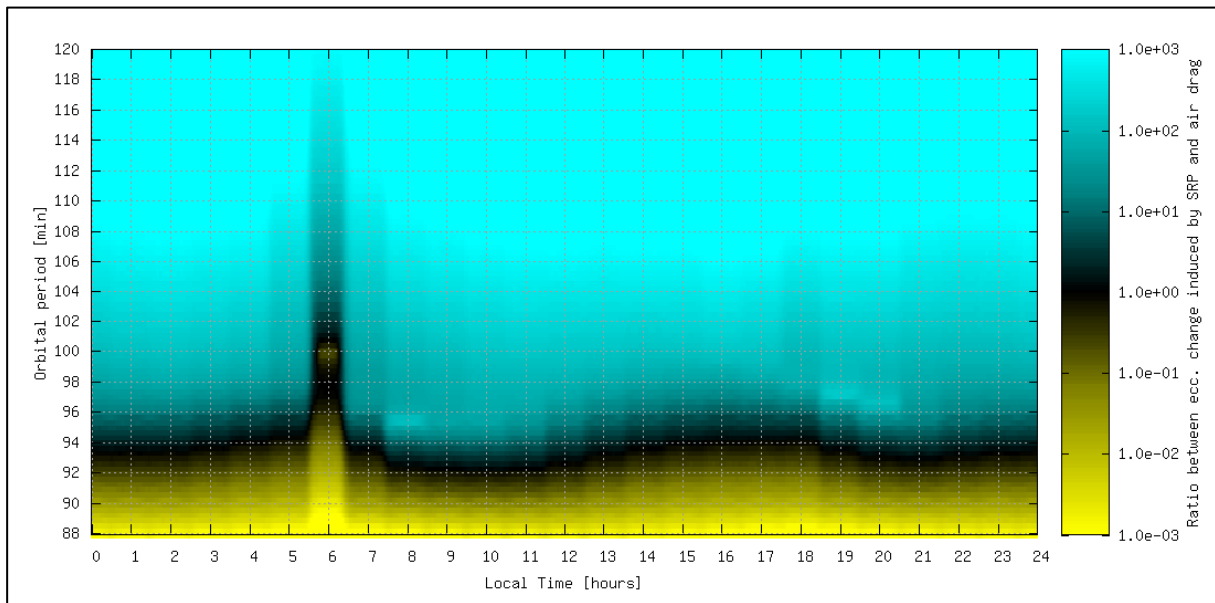


Fig. 7: Comparison of the eccentricity changes induced by air drag and SRP. Low solar activity scenario.

The data depicted in Fig. 5, Fig. 6 and Fig. 7 also shows a seasonal dependency. The main causes of this time dependency are the position of the Sun throughout the year with respect to the equatorial plane, the variation of the solar activity levels and other seasonal dependencies of the air drag force [6]. A detailed analysis of these characteristics is left as a possible further work on this topic.

A number of features can be identified in the data plotted in Fig. 5: Higher influence of air drag driven eccentricity changes for orbital plane orientations close to 6 and 18 hours; local maxima and minima of Eqn 5 for isolated points (e.g. Maxima: local time 8 hours, orbit period 103 minutes; local time 19 hours, orbit period 107 minutes. Minimum: local time 6 hours, orbit period 100 min). The clarification of these characteristics requires a closer look at the numerator and denominator of the quotient defined in Eqn 5.

Fig. 8 shows the magnitude of eccentricity changes caused by the SRP as a function of the orbital period and the local time. It can be seen that the eccentricity change induced by SRP is minimum for local times of 6 and 18 hours. This is due to the fact that at these orbital plane orientations the projection of the SRP force onto the orbital plane reaches a minimum value. An increase in the eccentricity change induced by SRP can also be observed as the orbital period increases. This is in line with the model given Eqn 1, which predicts an increase as the semi-major axis grows and the arc length covered by eclipse decreases. The same data has been depicted in Fig. 9 using logarithmic scale, in which a near cancellation of the SRP effect for a local time of 6 hours and an orbital period of approximately 100 minutes can be observed. The orbital period for which this occurs varies with the date. The inclination for a 100-minute sun-synchronous orbit is such that the SRP direction is perpendicular to the orbital plane. The case in the plot corresponds to the 1st of September, where the Sun elevation above the equatorial plane is 8.433 deg, and the inclination of a sun-synchronous orbit with 100 minutes period is 98.433 deg. This results in the minimum observed in Fig. 9.

Likewise, the eccentricity change induced by air drag has been depicted in Fig. 10 and Fig. 11 using a linear and a logarithmic scale respectively. Minimum values can be observed as well in Fig. 11 at local time 19 hours with an orbital period of 107 minutes, and local time 8 hours with an orbital period of 103 minutes. These cases correspond to particular density distribution along

the orbit, which are fully balanced in the sense introduced in Fig. 1. These cases result in a null eccentricity change caused by air drag.

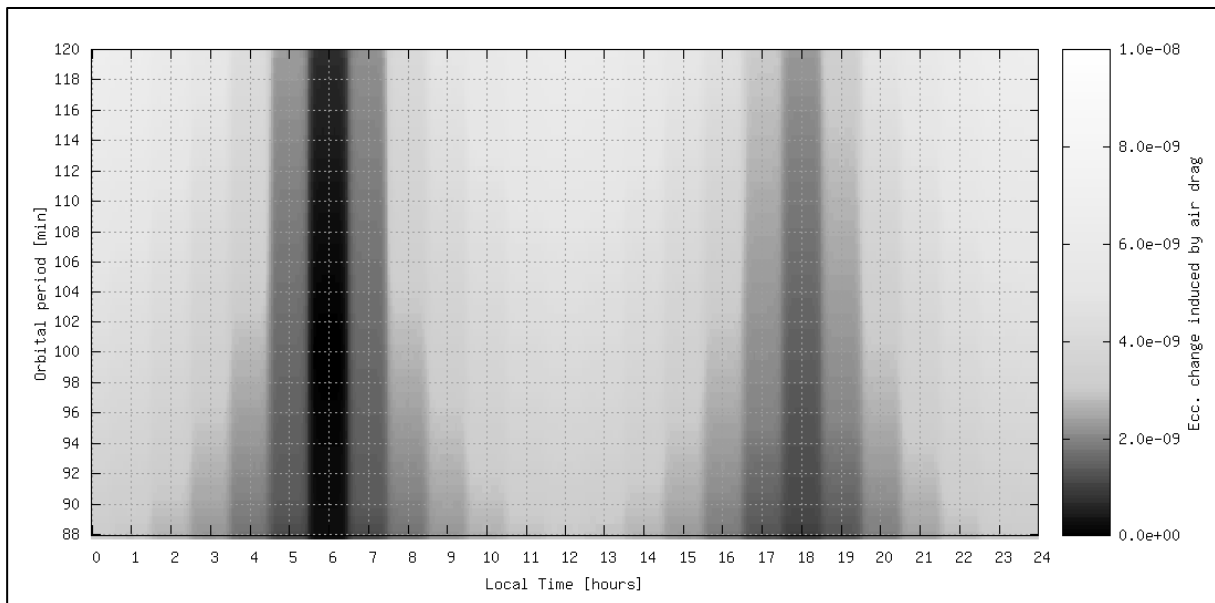


Fig. 8: Magnitude of eccentricity changes induced by SRP.

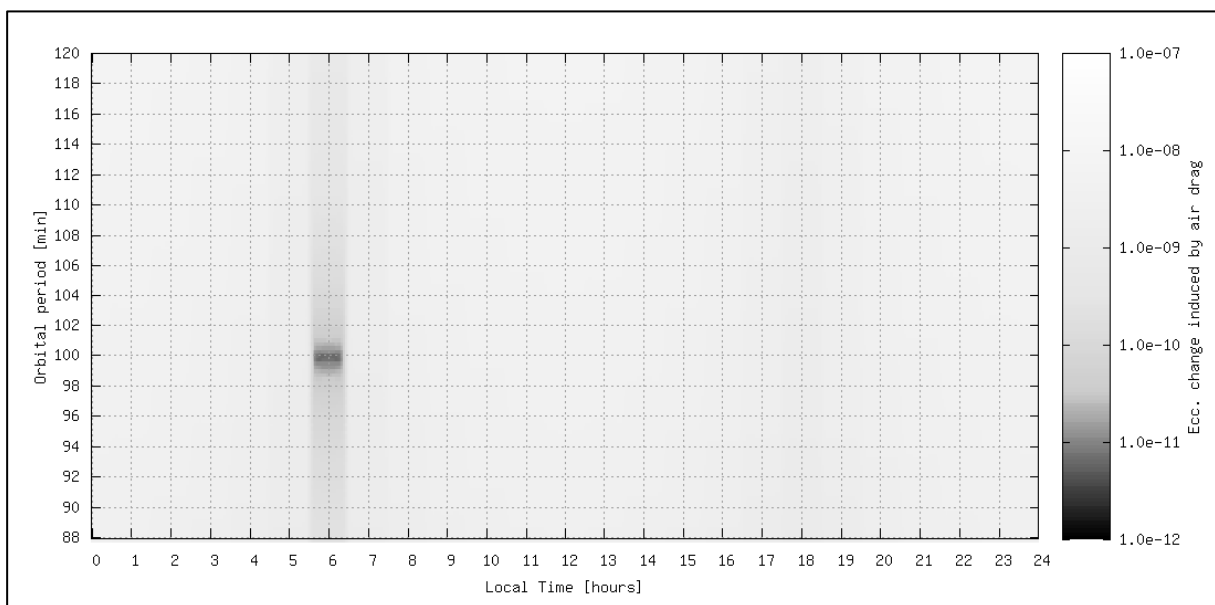


Fig. 9: Magnitude of eccentricity changes induced by SRP. Logarithmic scale.

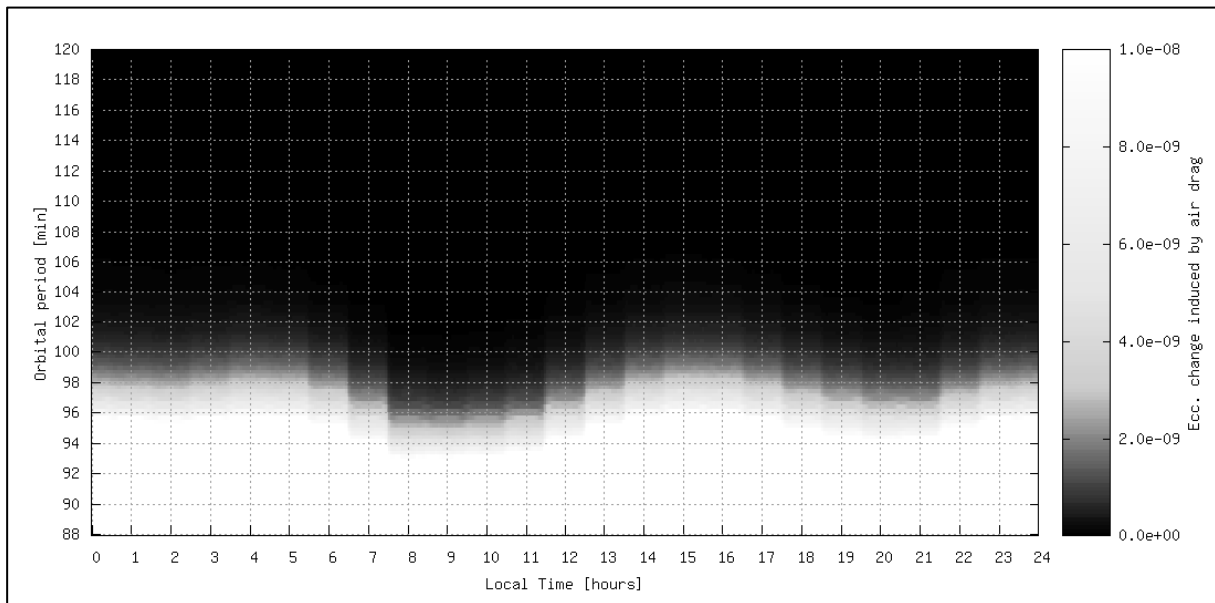


Fig. 10: Magnitude of eccentricity changes induced by air drag.

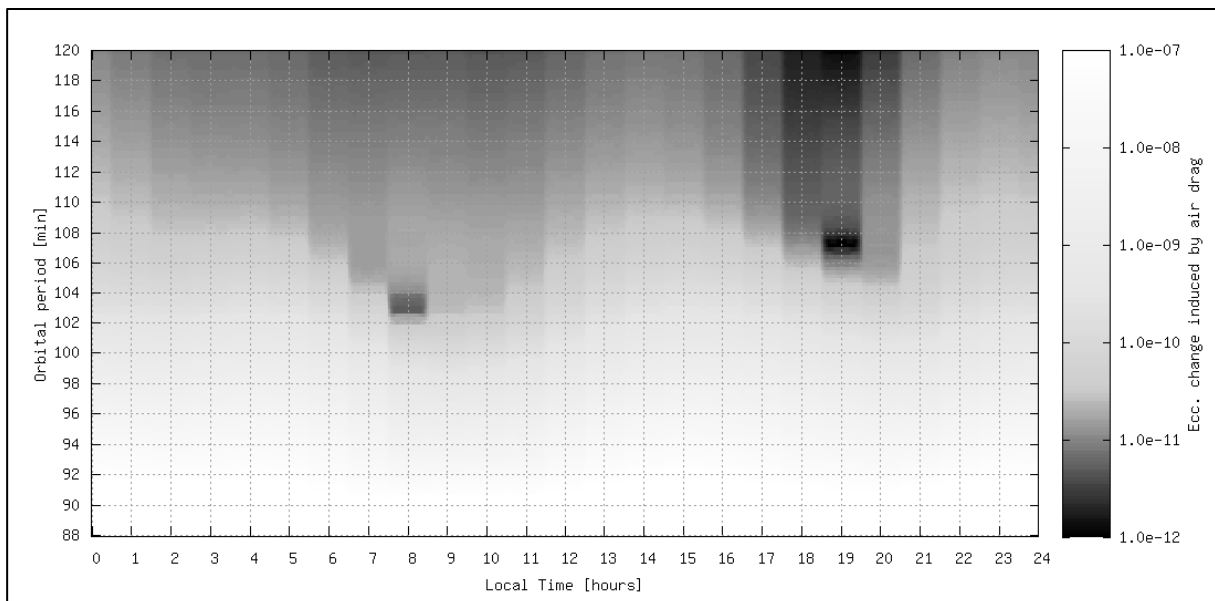


Fig. 11: Magnitude of eccentricity changes induced by air drag. Logarithmic scale.

Conclusions

A study on the disturbances in the eccentricity vector caused by air drag has been carried out. The method used to evaluate eccentricity changes caused by the air drag perturbation has been introduced. It makes use of the variational equations in the Gauss form integrating the effect of the air drag force in the eccentricity vector. It has been observed that the unevenness in the air drag distribution along the orbit causes net changes in the eccentricity vector. Depending on the orbit characteristics these eccentricity changes may not be negligible with respect to the ones caused by other perturbations like the SRP. This was illustrated with orbits at the altitude and orbital plane orientation of the ESA missions Sentinel-3 and Aeolus.

Then, a comparison of eccentricity changes caused by SRP and air drag has been made for near-circular sun-synchronous orbits, as a function of their local time and altitude, covering the range of orbital periods from 88 minutes to 120 minutes. The results of the analysis allow determining which perturbation dominates the dynamics in the eccentricity vector.

Further work on this topic may focus on the seasonal variability of air drag driven eccentricity changes, a characterisation of the direction of the eccentricity changes as a function of the orbit characteristics, or specific application to the eccentricity control of particular missions, with air drag dominated eccentricity changes (e.g. Aeolus or EarthCARE).

References

1. Sánchez, J., Martín Serrano, M.A. and Mackenzie, R., “Characterization of the Solar Radiation Pressure Perturbation in the Eccentricity Vector”. Proceedings 25th International Symposium on Space Flight Dynamics - 25th ISSFD. Munich, Germany, 2015.
2. Sánchez, J., Kuchynka, P., “Analysis of the Eccentricity Vector in Low Earth Orbits as Planar Rigid Body Motion”. Proceedings 26th International Symposium on Space Flight Dynamics - 26th ISSFD. Matsuyama, Japan, 2016.
3. Rosengren, M., “Improved Technique for Passive Eccentricity Control” American Astronautical Society Publication, AAS-89-155, 1989.
4. Dennis D. McCarthy (ed.). “IERS Standards (1989). (IERS Technical Note ; 3). Chapter 14: Radiation Pressure Reflectance Model” Paris: Central Bureau of IERS - Observatoire de Paris, 1989. iv, 77 p.
5. Vallado, D.A., “Fundamentals of Astrodynamics and Applications”. Space Technology Library. Springer (2007), ISBN 0-7923-6903-3.
6. Qian, L., Solomon, S.C. and Kane, T.J., "Seasonal variation of thermospheric density and composition". Journal of Geophysical Research, Vol. 114, A01312, doi: 10.1029/2008JA013643, 2009.